Optics Letters

Optical path difference microscopy with a Shack–Hartmann wavefront sensor

Hai Gong,[1,*] Temitope E. Agbana,[1] Paolo Pozzi,[1] Oleg Soloviev,[1,2,3] Michel Verhaegen,[1] and Gleb Vdovin[1,2,3]

[1]*Delft University of Technology, Mekelweg 2, 2628 CD Delft, The Netherlands*
[2]*Flexible Optical B.V., Polakweg 10-11, 2288 GG Rijswijk, The Netherlands*
[3]*ITMO University, Kronverksky 49, 197101 St. Petersburg, Russia*
Corresponding author: h.gong@tudelft.nl

In this Letter, we show that a Shack–Hartmann wavefront sensor can be used for the quantitative measurement of the specimen optical path difference (OPD) in an ordinary incoherent optical microscope, if the spatial coherence of the illumination light in the plane of the specimen is larger than the microscope resolution. To satisfy this condition, the illumination numerical aperture should be smaller than the numerical aperture of the imaging lens. This principle has been successfully applied to build a high-resolution reference-free instrument for the characterization of the OPD of micro-optical components and microscopic biological samples. © 2017 Optical Society of America

Optical path difference (OPD) is an important modality in modern microscopy, as it provides additional information about the structure of microscopic samples, especially when the intensity modulation is weak due to low absorption in the specimen. In many cases, such as the characterization of micro-optical components, it is important to measure the quantitative distribution of the sample OPD, with a precision comparable to ordinary optical shop testing.

Phase contrast microscopy visualizes the OPD of microscopy samples, and different techniques can be used to achieve this phase contrast. Zernike phase contrast microscopy increases the image contrast by manipulating the phase difference between the scattered and unscattered light [1,2]. However, this intensity information cannot be converted to OPD directly; moreover, the images are affected by an inherent halo and shade-off artifacts. Differential interference contrast microscopy is a kind of shearing interferometry that generates the phase gradient contrast by slightly shifting two polarized light beams and then having them interfere with each other [3]. This method is more popular than Zernike phase contrast for its good pseudo three-dimensional view and improvement on the transverse resolution, although

it cannot be employed to quantitative OPD measurements due to its nonlinear response [4].

Interferometric methods, such as interference microscopy and digital holographic microscopy, provide quantitative phase measurements with high transverse resolution [5], but they require a highly coherent light source. On the other hand, white-light interferometry usually requires an accurate positioning stage to achieve quantitative measurements [6]. In addition, the practical applicability of these interferometric methods is limited by the requirements of a highly coherent reference beam [7,8].

Phase diversity methods [9,10] retrieve the phase by iteratively solving inverse problems using a well-established diffraction theory. Mostly, they suffer from slow convergence and non-uniqueness due to the ill-posed nature of the problem. Redundant constraints, such as intensity measurements at different distances [11], with diverse phases [12] and with varying apertures [13,14], can be used to improve phase retrieval performance. The additional apparatus required by these methods further complicates the imaging system.

Wavefront sensing technology is widely and maturely developed in the field of adaptive optics [15]. A quadriwave lateral shearing interferometry wavefront sensor has been employed for quantitative phase imaging and has achieved a sensitivity of a few nanometers [16]. Recently, a technique named partitioned aperture wavefront sensing also realized a quantitative phase measurement with incoherent illumination by using a quatrefoil lens [17].

Shack–Hartmann (SH) wavefront sensors are widely used to detect the smooth wavefronts of the light beam. Such a restriction to low-order reconstruction is sufficient for many applications; thus, the transverse resolution of SH sensors was inferior to the interferometric and phase retrieval sensors [18]. However, the development of high-resolution SH sensors facilitates their direct application to imaging problems, for example, a holographic imaging with a SH sensor has been recently demonstrated: [19].

In this Letter, we report a quantitative OPD microscope based on a high resolution SH wavefront sensor. By directly using wavefront reconstruction technique, the OPD due to the sample thickness and refractive index can be simply obtained by integration of the gradient field registered by the

sensor. This non-interferometric technique is able to work under spatial incoherent illumination with high light efficiency. As a widely available optical component, the SH wavefront sensor can easily transform an ordinary microscope into an OPD imaging modality with the following described principles.

The scheme of the SH-based OPD microscope is shown in Fig. 1. To correctly understand its function, we need to consider two optical paths. (1) The imaging is performed by projecting the sample image on the microlens array (MLA) by the optical system formed by the objective lens and the tube lens with magnification $M = f_t/f_o$, where f_t and f_o are the focal lengths of the tube and the objective lens, respectively. In this optical path, each lenslet corresponds to a single pixel in the image of the sample intensity. (2) The wavefront sensing path is formed by the light source, a transparent sample with unknown OPD distribution, an objective lens, a tube lens, and a MLA. The first image of the light source is formed in the pupil of the objective lens if $L \gg f_o$ which is easy, considering the short focal length of microscope objectives. The position of this image depends on the wavefront tilts introduced by the sample. The pupil plane, containing an image of the source, is conjugated to the image sensor by the system formed by the tube lens and one of the lenslets. Since each lenslet corresponds to a single resolution point in the sample plane, the lateral shift of the source image behind the lenslet will be dependent on the local wavefront tilt introduced in the corresponding point of the sample.

To obtain a correct SH pattern with localized light spots, the position of which is linearly dependent on the OPD gradients, two physical conditions should be satisfied:

(1) To guarantee that the scattered light has enough space to move in the pupil of objective, the half angular size of the light cone α scattered by the sample should be smaller than the aperture angle of the objective:

$$\tan(\alpha) \ll A_o. \tag{1}$$

(2) To guarantee the correct centroiding, the image of light source behind the lenslet should be smaller than the MLA pitch:

$$\tan(\alpha/M) \ll A_M, \tag{2}$$

where A_M is the numerical aperture of the micro-lens array.

With the assumption that the sample has a minor effect on the scattered light cone, the angle α is mainly defined by the numerical aperture of the illumination A_s. According to Van Cittert–Zernike theorem, the coherence size provided by an extended source with a numerical aperture of A_s in the plane of
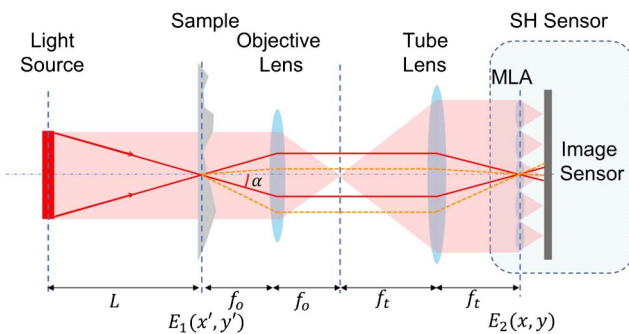
the sample is proportional to $\sim \lambda/A_s$, while the resolution of the microscope is defined by the numerical aperture of the imaging lens $\sim \lambda/A_o$. This brings us to a conclusion that, to secure correct operation of a SH sensor, the length of spatial coherence of the illumination light in the sample plane should be larger than the optical resolution of the microscope. In the plane of the MLA, full spatial resolution is obtained with lenslets that are smaller than the microscope point spread function (PSF). This condition is equivalent to the requirement of complete spatial coherence over the extent of a single lenslet. If the lenslet size is larger than the PSF size, correct wavefront reconstruction is still possible, with some loss of spatial resolution, as long as condition 2 is satisfied.

Compared to the usual wavefront sensing requirement of complete coherence over the whole aperture of the sensor, these requirements are much softer. This difference is explained by the fact, that the OPD function is a deterministic function which is coherent by definition; therefore, only local coherence of the probe light is needed to characterize it. In contrast, the wavefront characterization in the field of adaptive optics, the deterministic function describing the wavefront can be defined only if the light is coherent over the whole sensor aperture, including all lenslets.

In the MLA plane, the wavefront gradient decreases by a factor of M due to the microscope magnification, while the wavefront height remains the same. The registered SH pattern can be approximated as a regular foci grid modulated by the wavefront gradients $\frac{\partial W}{\partial x}, \frac{\partial W}{\partial y}$ under the assumption that the spots are circularly symmetric and equal. The wavefront gradients may be retrieved from the first harmonics as follows [20,21]:

$$I_{SH}(x,y) = E_2(x,y)E_2^*(x,y)\left\{2 + \cos\left[\frac{2\pi}{P}\left(x + F\frac{\partial W}{\partial x}\right)\right]\right.$$
$$\left. + \cos\left[\frac{2\pi}{P}\left(y + F\frac{\partial W}{\partial y}\right)\right]\right\}, \tag{3}$$

where F is the focal length of a lenslet. P is the pitch of MLA. Therefore, the illumination source should also meet the same requirement as the assumption for SH spots. When considering the absorption of the sample, the movement of spots is not affected by small intensity variations. If the absorption is severe, however, the SH pattern should be carefully exposed or enhanced with high dynamic range techniques.

In this Letter, we retrieve the wavefront gradients by using the Fourier demodulation method [22]. A reference wavefront is registered in advance in the absence of a sample, for sensor calibration. Then the OPD gradients brought by the sample $\frac{\partial O(x,y)}{\partial x}, \frac{\partial O(x,y)}{\partial y}$ can be obtained by calculating the deviation from the reference. Finally, we can reconstruct the OPD by two-dimensional gradient integration [23]:

$$O(x,y) = \mathcal{F}^{-1}\left\{-i\frac{f_x\mathcal{F}\{\frac{\partial O(x,y)}{\partial x}\} + f_y\mathcal{F}\{\frac{\partial O(x,y)}{\partial y}\}}{f_x^2 + f_y^2}\right\}. \tag{4}$$

Here $\mathcal{F}\{\cdot\}$ and $\mathcal{F}^{-1}\{\cdot\}$ denote the Fourier transform and inverse Fourier transform. f_x, f_y are the coordinates in the frequency domain. Note that phase unwrapping is needed when the obtained wavefront gradients contain phase jumps [24].

To study the feasibility and accuracy of this method, the OPD profile of a microlens array (APO-Q-P300-R8.6, AMUS GmbH) was measured in the experiment with a customized microscope in the configuration of Fig. 1. The light source is a collimated LED (M470L3-C1, Thorlabs) with

Fig. 1. Diagram of the SH quantitative OPD microscope.

the central wavelength of 460 nm and a bandwidth of 25 nm. The numerical aperture of this collimated LED source is $A_s \approx 0.02$. A commercial SH sensor (FS3370-O-P63-F2, OKO Tech) consisting of 140×140 lenslets with a pitch of $P = 63$ μm, a focal length of $F = 2$ mm, with a 2048×2048 digital CMOS sensor was employed for image registration. Our setup is built to satisfy the condition

$$P \leq M \cdot \frac{\lambda}{A_o}, \tag{5}$$

which is equivalent to (2). According to Eq. (5), the microscope was then implemented with a 10× microscope objective ($A_o = 0.25$) and a tube lens with $f_t = 400$ mm, providing ~2.5× extra magnification, resulting in a total magnification of 25×. With a 63 μm lenslet, here we have experienced some loss in the spatial resolution, but the OPD was correctly reconstructed since condition 2 was still satisfied.

The experimental results are shown in Fig. 2. According to the manufacturer specification sheet, the sample lenslets have a plano–convex spherical shape with a pitch of 300 μm and a nominal focal length of 18.6 mm. The sagitta of the microlens is $s = 1.31$ μm. The contrast of the bright field image in Fig. 2(a) is very poor, even though some ring structures are visible. Figure 2(b) shows the three-dimensional reconstruction of the OPD in the specimen. The layer structure due to the lithographic fabrication process is clearly visible. The refractive index of the central wavelength in the fused silica is $n = 1.4647$. Then the OPD map of a single microlens is converted to the optical thickness in Fig. 2(c). The blue line in Fig. 2(d) is the center line cross section of the microlens thickness map. The measured sagitta $s = 1.388$ μm is close to the given geometric parameter. The red dashed line is the measurement of the same microlens in the same setup, but with the LED replaced by a collimated fiber laser (HLS635, Thorlabs). The wavelength of the laser is 635 nm, and the refractive index is then $n = 1.4570$. We can see a very good
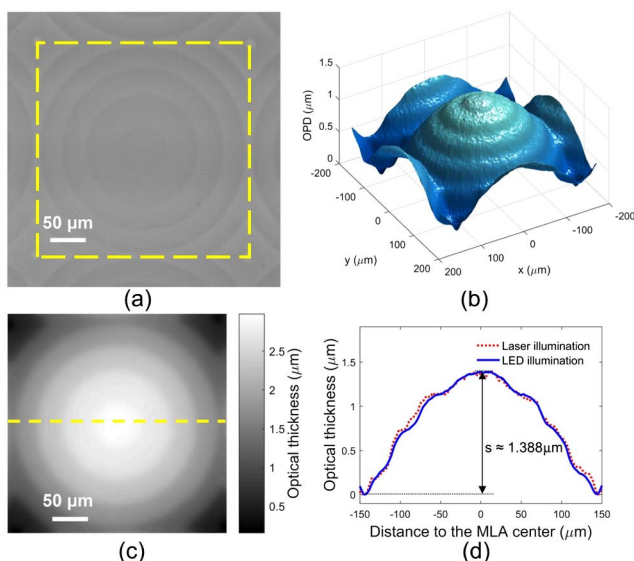
agreement between these two measurements. The variance may be due to the speckle noise, as it tends to produce a more noisy measurement, compared to partially coherent light. The spatial resolution in this particular case is limited to $r_s = P/M \approx 2.5$ μm. In the assumption of noiseless registration, the OPD error per lenslet can be derived from the average wavefront curvature over the lenslet $\Delta_M \approx r_s^2 \overline{|\frac{d^2\psi}{dr^2}|}$, where ψ is the OPD function and r is the coordinate. For a spherical surface with radius R we have $\overline{|\frac{d^2\psi}{dr^2}|} = 1/R$. In this particular case, with $R = 18.6$ mm, $\Delta_M \approx 0.34$ nm. Further analysis of the OPD error due to reconstruction noise, speckle, sensor sensitivity, and other factors, is out of scope of this work. The data of our reconstruction, including thickness and number of layers, and the amplitude of the surface waviness, are in perfect agreement with the manufacturer's data, obtained independently for this particular sample (Leleko, private communication).

In Fig. 3, we investigated the influence of the illumination coherence on the accuracy of the OPD measurement. The incoherent LED illumination was scattered by a ground glass with a diameter of $D = 25.4$ mm at a distance L from the sample. We controlled the source angular size $A_s = D/2L$ by changing the distance L between the ground glass and the sample. The experiment produces correct reconstruction as long as the illumination size $A_s \leq 0.17$. A further increase of A_s causes the measurement error to rise quickly, when A_s is approaching A_o, in agreement with our analysis. The increase of the illumination NA results in a larger bright source image inside the dark objective lens pupil. Wavefront tilts are sensed as movements of this bright image in the dark field. When the source image becomes too large, wavefront tilts result in vignetting of the shifted image by the edges of the pupil, producing erroneous measurements. Finally, when the image is larger than the pupil, the sensitivity to movements is reduced to zero. In this configuration, condition 2 is always satisfied; therefore, some strongly scattered ray movements were still sensed. Thus, we have shown experimentally that a SH sensor can be used for precision measurements of OPD profiles with relatively low coherent illumination. Conventional microscopes could be easily converted for OPD imaging by properly adjusting the numerical aperture of the illumination system.

We have further applied this microscope to biological samples. An unstained dry red blood cell (RBC) smear was observed under a 40× objective (NA = 0.65). Figure 4 is the bright field image of RBCs. In this image, only the outline of the RBCs is visible. Details of the content of the RBCs, however, are invisible
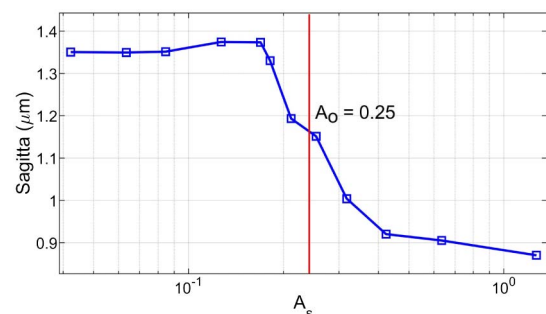
Fig. 2. (a) Bright field microscope of a lenslet obtained with a 10× microscope objective with $A_o = 0.25$. (b) 3D OPD map of the MLA reconstructed from a SH sensor with a LED illumination. (c) Thickness map of the lenslet. (d) Center cross section of the microlens reconstructed with LED and laser illumination.

Fig. 3. Measured thickness of the microlens sagitta versus the numerical aperture of illumination A_s.
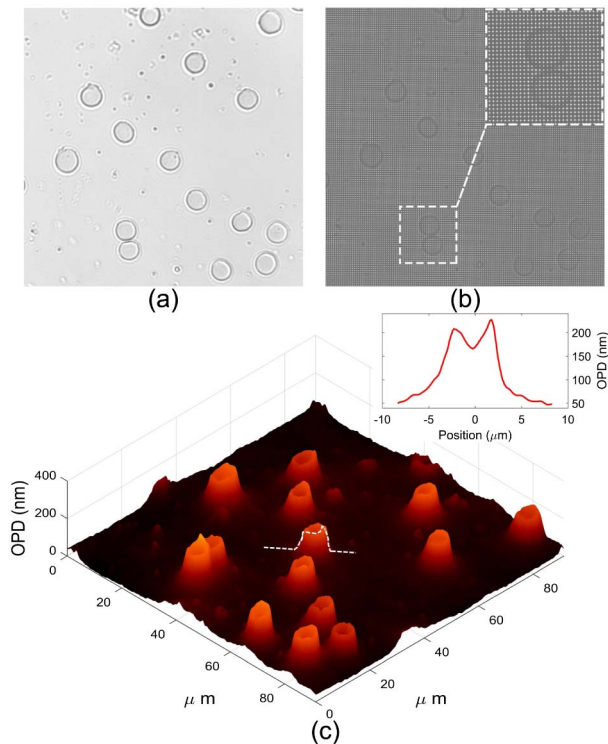
Fig. 4. (a) Bright field image of RBCs, (b) the SH pattern, and (c) the reconstructed OPD map. A ross session of the OPD of the individual blood cell is shown in the inset.

Fig. 5. OPD measurement of a living cheek cell: (left) the bright field intensity image; (right) the OPD map.

transmissive imaging cases have been verified in experiments, this technique holds potential for reflective surface profile imaging.

due to the transparency of the RBCs. The OPD map, shown in Fig. 4(c), offers more topographic information of the RBCs, e.g., the ring shape of blood cells. Thus, this method offers interesting potential for blood related disease diagnostics.

Figure 5 shows both the bright field image and an OPD map of a living human cheek cell. The sample was surrounded by physiological saline and was sandwiched between a microscope slide and a cover slip. The biological structure of the cheek cell, including the nucleus, cytoplasm, and membrane ruffles, is visible in the OPD map, while it is difficult to resolve from the bright field image without labeling. Benefiting from the high photon efficiency by using MLA to gather light, the SH image of the cell was acquired at an exposure time less than 5 ms which enables real-time cell and sub-cell activity monitoring.

In summary, we have shown that for instrumental application of a SH sensor to characterize the OPD of transparent samples in an imaging microscope, the lateral coherent length of the illumination should be larger than the resolution of the imaging lens of the microscope. Additionally, the numerical aperture of the illumination source should be smaller than the numerical aperture of the imaging lens. This condition allows one to optimize the microscope both for high-resolution imaging and for correct OPD sensing. Based on these principles, we have developed a simple and robust quantitative OPD imaging microscope with which we have accurately characterized the OPD profile of microscopic samples. This method can be easily applied to a conventional microscope, through proper alignment of the illumination setup, providing a low-cost methodology for quantitative OPD analysis. Although only
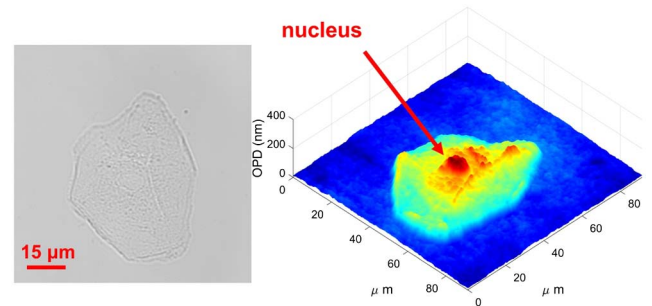
REFERENCES

1. F. Zernike, Physica **9**, 974 (1942).
2. D. B. Murphy, *Fundamentals of Light Microscopy and Electronic Imaging* (Wiley, 2002).
3. H. Gundlach, Opt. Eng. **32**, 3223 (1993).
4. C. Sheppard, *Phase Contrast Microscopy* (Elsevier, 2005).
5. M. K. Kim, *Digital Holographic Microscopy* (Springer, 2011).
6. J. C. Wyant, Proc. SPIE **4737**, 98 (2002).
7. P. Ferraro, S. De Nicola, A. Finizio, G. Coppola, S. Grilli, C. Magro, and G. Pierattini, Appl. Opt. **42**, 1938 (2003).
8. B. Kemper and G. von Bally, Appl. Opt. **47**, A52 (2008).
9. R. A. Gonsalves, Opt. Eng. **21**, 829 (1982).
10. Y. Shechtman, Y. C. Eldar, O. Cohen, H. N. Chapman, J. Miao, and M. Segev, IEEE Signal Process. Mag. **32**, 87 (2015).
11. C. Guo, C. Wei, J. Tan, K. Chen, S. Liu, Q. Wu, and Z. Liu, Opt. Lasers Eng. **89**, 2 (2017).
12. P. Gao, G. Pedrini, C. Zuo, and W. Osten, Opt. Lett. **39**, 3615 (2014).
13. H. Gong, P. Pozzi, O. Soloviev, M. Verhaegen, and G. Vdovin, Proc. SPIE **9899**, 98992N (2016).
14. H. Lu, J. Chung, X. Ou, and C. Yang, Opt. Express **24**, 25345 (2016).
15. R. K. Tyson, *Principles of Adaptive Optics* (CRC Press, 2015).
16. P. Bon, G. Maucort, B. Wattellier, and S. Monneret, Opt. Express **17**, 13080 (2009).
17. A. B. Parthasarathy, K. K. Chu, T. N. Ford, and J. Mertz, Opt. Lett. **37**, 4062 (2012).
18. J. Chanteloup, Appl. Opt. **44**, 1559 (2005).
19. H. Gong, O. Soloviev, D. Wilding, P. Pozzi, M. Verhaegen, and G. Vdovin, Opt. Express **24**, 13729 (2016).
20. Y. Carmon and E. N. Ribak, Opt. Commun **215**, 285 (2003).
21. C. Canovas and E. N. Ribak, Appl. Opt. **46**, 1830 (2007).
22. A. Talmi and E. N. Ribak, J. Opt. Soc. Am. A **21**, 632 (2004).
23. A. Talmi and E. N. Ribak, J. Opt. Soc. Am. A **23**, 288 (2006).
24. M. A. Herráez, D. R. Burton, M. J. Lalor, and M. A. Gdeisat, Appl. Opt. **41**, 7437 (2002).